Physics of Plasmas

RESEARCH ARTICLE | MAY 07 2025

Development of a high charge 10 GeV laser electron accelerator

Special Collection: Papers from the 66th Annual Meeting of the APS Division of Plasma Physics

E. Rockafellow ; B. Miao ; J. E. Shrock ; A. Sloss ; M. S. Le ; S. W. Hancock ; S. Zahedpour ; R. C. Hollinger ; S. Wang ; J. King ; P. Zhang ; J. Šišma ; G. M. Grittani ; R. Versaci ; D. F. Gordon ; G. J. Williams ; B. A. Reagan; J. J. Rocca ; H. M. Milchberg

Phys. Plasmas 32, 053102 (2025)
https://doi.org/10.1063/5.0265640

AIP Publishing

Physics of Plasmas ARTICLE pubs.aip.org/aip/pop

Development of a high charge 10 GeV laser electron accelerator

Cite as: Phys. Plasmas **32**, 053102 (2025); doi: 10.1063/5.0265640
Submitted: 14 February 2025 · Accepted: 7 April 2025 ·
Published Online: 7 May 2025

E. Rockafellow,[1] B. Miao,[1] J. E. Shrock,[1] A. Sloss,[1] M. S. Le,[1] S. W. Hancock,[1] S. Zahedpour,[2] R. C. Hollinger,[2] S. Wang,[2] J. King,[2] P. Zhang,[2] J. Šišma,[3,4] G. M. Grittani,[3] R. Versaci,[3] D. F. Gordon,[5] G. J. Williams,[6] B. A. Reagan,[6] J. J. Rocca,[2,7] and H. M. Milchberg[1,8,a)]

AFFILIATIONS

[1]Institute for Research in Electronics and Applied Physics and Department of Physics, University of Maryland, College Park, Maryland 20742, USA
[2]Department of Electrical and Computer Engineering, Colorado State University, Fort Collins, Colorado 80523, USA
[3]ELI Beamlines Facility, The Extreme Light Infrastructure ERIC, Dolni Brezany 25241, Czech Republic
[4]Faculty of Nuclear Sciences and Physical Engineering, Czech Technical University in Prague, Brehova 7, 11519 Prague, Czech Republic
[5]Naval Research Laboratory, Washington, DC 20375, USA
[6]Lawrence Livermore National Laboratory, Livermore, California 94550, USA
[7]Department of Physics, Colorado State University, Fort Collins, Colorado 80523, USA
[8]Department of Electrical and Computer Engineering, University of Maryland, College Park, Maryland 20742, USA

Note: This paper is part of the Special Collection: Papers from the 66th Annual Meeting of the APS Division of Plasma Physics.
[a)]**Author to whom correspondence should be addressed:** milch@umd.edu

ABSTRACT

Low-density meter-scale plasma waveguides produced in meter-scale supersonic gas jets have paved the way for recent demonstrations of all-optical multi-gigaelectronvolt laser wakefield acceleration (LWFA). This paper reviews recent advances by the University of Maryland, which have enabled these results, focusing on the development of elongated supersonic gas jets up to ~ 1 m in length, experimental and simulation studies of plasma waveguide formation, and a new three-stage model for relativistic pulse propagation dynamics in these waveguides. We also present results from recent LWFA experiments conducted at the Laboratory for Advanced Lasers and Extreme Photonics at Colorado State University demonstrating high charge, low divergence electron bunches to ~ 10 GeV, with laser-to-electron beam efficiency of at least $\sim 30\%$.

I. INTRODUCTION

Compact, laser-plasma particle accelerators have recently been employed as drivers for secondary light sources[1,2] and free electron lasers,[3] and offer a possible path toward future high-energy colliders.[4] Laser wakefield acceleration (LWFA)[5,6] harnesses the strong electrostatic fields of laser-driven plasma waves to achieve extremely strong accelerating gradients $\sim 10^3$ times greater than those of rf accelerators, enabling the production of multi-gigaelectronvolt (GeV) electron bunches over sub-meter distances.[7–15] For petawatt-class lasers, maximizing energy gain in an LWFA requires accelerating electrons over tens of centimeters—much further than the natural diffraction scale of an ultra-intense laser pulse focused to $<100\,\mu$m spot size.[5,7,16] Thus, some form of optical guiding is required to maintain sufficient intensity for wake excitation over the full length of the accelerator.

Relativistic nonlinear self-guiding has generated multi-GeV electron bunches,[10,11,14] but this approach is inefficient, demanding petawatt laser powers[10,11] for the low $\sim 10^{17}$ cm^{-3} plasma densities needed to achieve multi-GeV acceleration by mitigating dephasing between the drive laser and the electron bunch.[7] Moreover, the reliance on nonlinearity limits the control of the acceleration process.

Preformed plasma waveguides act as optical fibers for intense laser pulses,[7–9,13,15,17–32] maintaining relativistic intensities for long distances (tens to hundreds of Rayleigh ranges), and offer new degrees of freedom for controlling this extended relativistic interaction, including control of optical modes and their group velocities.[9,19,33] The first experimental demonstration of preformed plasma waveguides[21,22] relied on 100 ps J_0 Bessel beam ionization and heating of extended plasma columns via inverse bremsstrahlung (IB) to drive a blast-wave expansion, with the reduced on-axis plasma density forming the high index "core" of the waveguide, and the high electron density cylindrical shock forming the low-index "cladding." Waveguides formed through this process enabled the detailed experimental and theoretical study of their quasi-bound mode structure[24,34–36] and made possible the first LWFA results in a plasma waveguide.[37] However, IB heating efficiency limited the waveguide plasma density to $\gtrsim 10^{19}$ cm^{-3}, two orders of magnitude greater than the desired range for multi-GeV LWFA. Plasma waveguides formed through an electrical discharge in a narrow capillary tube of several hundred micrometers diameter[25,38,39] have also been applied to LWFA, though the fixed relationship between capillary geometry, waveguide optical properties, and on-axis density[13,37,40–42] makes reaching waveguide plasma densities $\sim 10^{17}$ cm^{-3} extremely challenging. One solution was presented in Refs. 13 and 42, where the use of auxiliary laser heating of a capillary plasma enabled plasma density reduction to $\sim 3 \times 10^{17}$ cm^{-3} and electron acceleration up to 7.8 GeV with 850 TW laser power. In addition, unlike capillary plasmas, laser-generated plasma waveguides are free-standing and immune to laser damage.

More recently, plasma waveguides formed by the hydrodynamic expansion of optical field ionized (OFI) plasmas[7–9,15,17,18,20,26–32,43] have enabled direct access to the low-density regime. However, OFI plasmas, say in hydrogen, have maximum electron temperatures of ~ 10 eV[18,20] while IB plasmas can have temperatures 10× higher. As a result, a single Bessel beam pulse is insufficient to generate the plasma cladding, requiring auxiliary pulses to ionize the high-density region surrounding the plasma core. For generating plasma cladding over meter scales, there are two techniques, the "2-Bessel" method[8,17] and "self-waveguiding."[7,18,32,44]

These new optical techniques for meter-scale waveguide formation,[17,18,32] along with our development of meter-scale supersonic gas jets,[7,8,17,19] enable an unprecedent degree of control over waveguide optical properties at the low plasma densities suitable for multi-GeV LWFA. The self-waveguiding and 2-Bessel techniques require phase front correction to produce high-fidelity zero-order and higher-order Bessel beams[8,45] focused into the extended gas sheets produced above the gas jets. The self-waveguiding method in a 20 cm hydrogen plasma waveguide[7,8] was soon employed in the first all-optical, multi-GeV LWFA experiment, accelerating electrons to 5 GeV using <300 TW. Since this initial demonstration, there have been rapid improvements in electron beam quality and energy, with the most recent experiments discussed in this article producing electron beams with over a nano-Coulomb of charge above 1 GeV, and electron bunch energies up to ~ 10 GeV.

In this paper, we review the developments leading to these results, starting with an overview of the University of Maryland's (UMd) meter-scale supersonic jet development. This is followed by a discussion of the most comprehensive experimental and simulation work conducted to date benchmarking meter-scale Bessel beam-generated OFI plasma waveguides.[20] We then introduce a three-stage model for relativistic pulse propagation in meter-scale low-density waveguides, highlighting a new universal mode beating effect that arises at high laser intensities and plays a critical role in laser propagation and ionization injection.[9] We present new experimental results, featuring the consistent and efficient production of multi-GeV LWFA electron bunches with energies to ~10 GeV, nC-level charge above 1 GeV, and sub-milliradian divergence. These experiments, conducted with laser energies of <18 J (<400 TW), achieve a laser-to-electron energy conversion efficiency of at least 30%.[46] Finally, we discuss our recently developed modular gas jet, in which waveguides extending >1 m can be generated with customizable density profiles. We present simulations showing improved acceleration using axially stepped waveguides that can be generated in these jets.

II. DEVELOPMENT OF METER-SCALE SUPERSONIC GAS JETS

Multi-GeV LWFA experiments require elongated, low-density plasmas. While gas cells[47–49] and capillary discharges[12,13,25] have been used in ~1 GeV[43] and multi-GeV LWFA experiments,[12,13] they lack accessibility for diagnostics, are highly susceptible to laser or discharge damage (thus limiting their repetition rates), and, in the case of capillaries, are unable to reach densities low enough ($N_{e0} \sim 10^{17}$ cm^{-3}) to mitigate dephasing.[7] Gas jets, however, do not have these limitations.

Gas jets have been developed in the Laboratory for Intense Laser Matter Interactions at the University of Maryland for many years, including those for IB-heated plasma waveguide generation,[50] elongated cluster jets for increased heating efficiency, and for generating axially modulated guides for application to direct laser acceleration[51–55] and thin, near-critical density jets for kHz LWFA using few-cycle millijoule pulses.[56] All of these jets were centimeter-scale or shorter. The first generation of elongated supersonic gas jets designed at Maryland was used to demonstrate the 2-Bessel method for OFI plasma waveguide generation.[17] This Mach 4 ($M = 4$) supersonic gas jet was 5 cm long, producing a smooth axial profile with measurable on-axis plasma waveguide densities as low as $N_{e0} \sim 10^{16}$ cm^{-3}.[17] One hydrogen backed solenoid valve (Parker series 9) fired into a reservoir-backed de Laval slit nozzle, which directed the gas upward in a sheet. This jet was re-designed and lengthened to 10 cm (Gen. II), fed by two similar valves and employed for direct characterization of the self-waveguiding process.[18]

To achieve 5 GeV in the first all-optical multi-GeV LWFA,[7] two design iterations were required, leading to our 20 cm, $M = 4$, Gen. IV jet, backed by 5 solenoid valves. We used a 95% H_2/5% N_2 (by number density) gas mix, with the waveguide generated by self-waveguiding in a channel generated 3 mm above the jet orifice by a zeroth order Bessel beam. The 5% N_2 dopant was used for ionization injection.[7,57–59] This jet also had a ~5 mm dopant injector section at the jet entrance backed by a sixth valve, although initial ionization injection attempts were hampered by a large-amplitude pulse deformation from mode beating at the guide entrance.[9] This experiment led to further refinements, including (1) operating at a higher Mach number to enable waveguide generation even farther from the orifice to avoid obstruction of the Bessel beam,[60] and (2) improving the design for the localized injector. This, with two more iterations, led to our 20 cm, $M = 5$, Gen. VI jet, backed by 6 solenoid valves, giving waveguide on-axis densities $N_{e0} \sim 1.5 \times 10^{17}$ cm^{-3} at 1.2 cm above the orifice, and localizing the N_2 dopant to a ~2 cm axial region at up to 5 evenly spaced locations along the 20 cm jet (the injector inlets were just below the nozzle). This resulted in quasi-monoenergetic <10% (resolution-limited) energy spread multi-GeV electron bunches.[9]

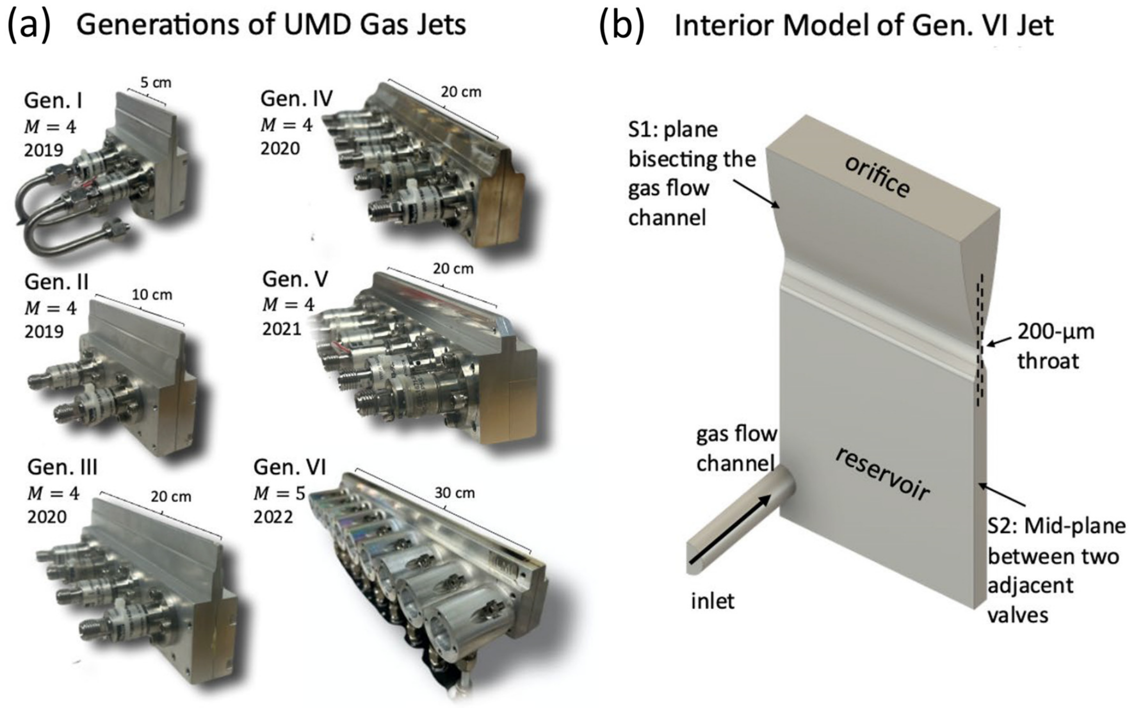

FIG. 1. University of Maryland supersonic gas jets. (a) Evolution of UMd gas jets ranging from a 5 cm jet designed in 2019 (Gen. I) to a 30 cm jet designed in 2022 (Gen. VI). (b) The internal structure of the Gen. VI jet, comprised of a reservoir to flatten the final density profile, a throat to determine the Mach number, and an orifice out of which the gas exits the jet in a longitudinal sheet.

For the 10 GeV result discussed below, the waveguide was formed in a 30 cm version of the $M = 5$ Gen. VI jet, backed by 9 solenoid valves (Parker C21). An internal longitudinal section of this jet [used for 3D fluid simulations[19] using Ansys Fluent with the shear-stress transport (SST) k–ω model[61]] is shown on the right side of Fig. 1. As in all of our jets, the "reservoir" smooths the longitudinal density profile, which otherwise would have peaks centered near each gas inlet. The 20 and 30 cm Gen. VI jets were used for the LWFA experiments discussed in this paper. Further details on this jet can be found in Ref. 19.

III. BENCHMARKING OF HYDRODYNAMIC PLASMA WAVEGUIDES

Optimizing LWFA in low-density meter-scale plasma waveguides requires detailed experimental characterization and modeling of the waveguide formation process. At low densities, the lower temperature Bessel beam-heated OFI plasma forms the waveguide core, with a weak or nonexistent plasma cladding. The role of the auxiliary 2-Bessel[17] and self-waveguiding[18] techniques is to ionize the neutral gas shock surrounding the plasma core to form a cladding. Thus, time-resolved measurements of the hydrodynamic evolution of both electron and neutral density profiles are crucial. Two-color interferometry measures the contribution of both electrons and neutrals to the refractive index profile.[18,20] For sufficient magnification to see waveguide features on the tens of micrometers scale, the interferometer transverse field of view is necessarily limited to a few millimeters at most. For meter-scale waveguides, such measurements are concatenated over small ranges <1 cm by shifting the object field over multiple shots. However, for practical measurements of meter-scale waveguides, we conduct transverse interferometry at a single position and then use longitudinal interferometry and fluorescence measurements (calibrated with H_2 backfill) to determine the average density and axial density variation.[7,8] The measurement is absolutely calibrated by measuring fluorescence from Bessel beam heating of backfill gas in the chamber at known pressures.

The hydrodynamically evolving channels in these measurements were generated with a diffractive axicon to form a J_0 Bessel beam pulse ($\lambda = 800$ nm, $\tau = 50$ fs FWHM, energy 150 mJ or 300 mJ, $R = 2$ cm beam radius, and Bessel beam axis approach angle $\gamma = 2.3°$) with either linear polarization (LP) or circular polarization (CP). Two-color interferometry used a spatially filtered, 800 nm beam, split pre-compression from the main beam and compressed separately to <100 fs. This pulse was frequency doubled with a 1 mm thick beta-barium borate (BBO) crystal to form a two-color (400 and 800 nm) probe beam, which was then passed through a $\Delta t = 0 - 10$ ns delay line before being transversely propagated through the plasma and directed into separate interferometers. Coincident electron and neutral density profiles were then extracted from the phase shift images in each color.[18,20] Figure 2 plots electron density [Figs. 2(a) and 2(b)] and neutral density [Figs. 2(a′) and 2(b′)] profile evolution after ionization of hydrogen gas by the LP or CP J_0 beam. Importantly, the interferometry measurements reveal that the electron density [Figs. 2(a) and 2(b)] peaks on-axis and then subsides over time, forming the plasma core but never forming the cladding necessary for a plasma waveguide. However, ionization of the neutral density shock [Figs. 2(a′) and

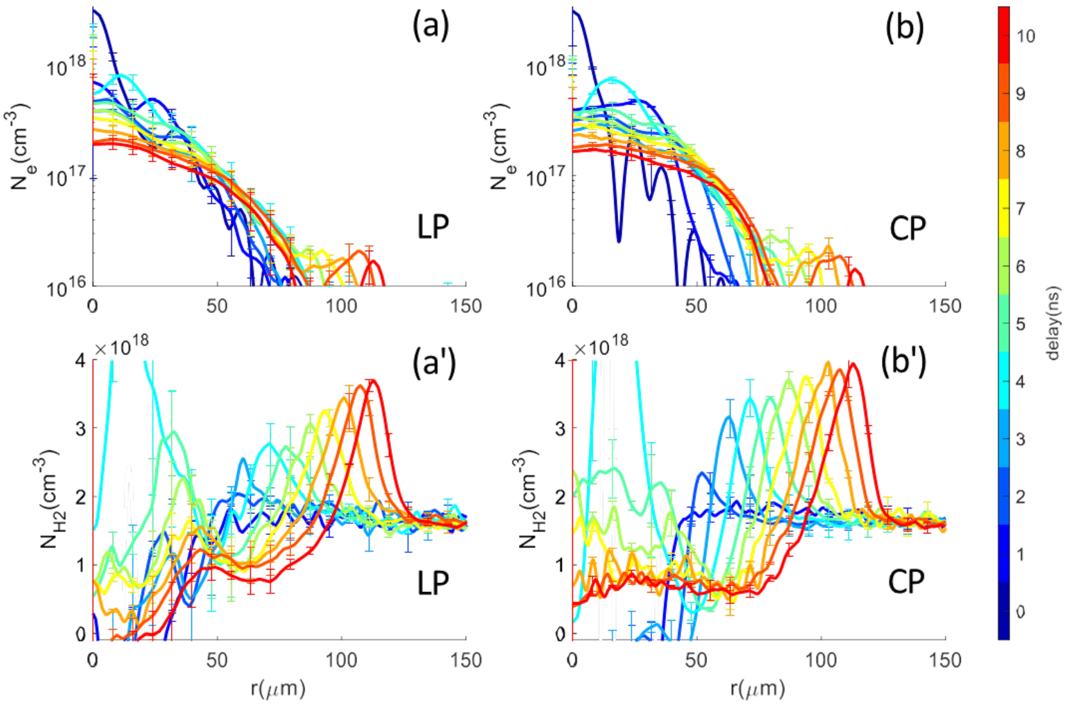

FIG. 2. Density profile temporal evolution of electron [(a) and (b)] and neutral hydrogen [(a′) and (b′)] for delays $\Delta t = 0 - 10$ ns for $\varepsilon_{Bessel} = 150$ mJ, beam radius 2 cm, pulse width 50 fs, and Bessel beam approach angle $\gamma = 2.3°$. (a) Linear polarization (LP) generated electron density profiles $N_e(r, \Delta t)$. (b) Circular polarization (CP) generated electron density profiles $N_e(r, \Delta t)$. (a′) LP-generated neutral hydrogen density and (b′) CP- generated neutral hydrogen density.

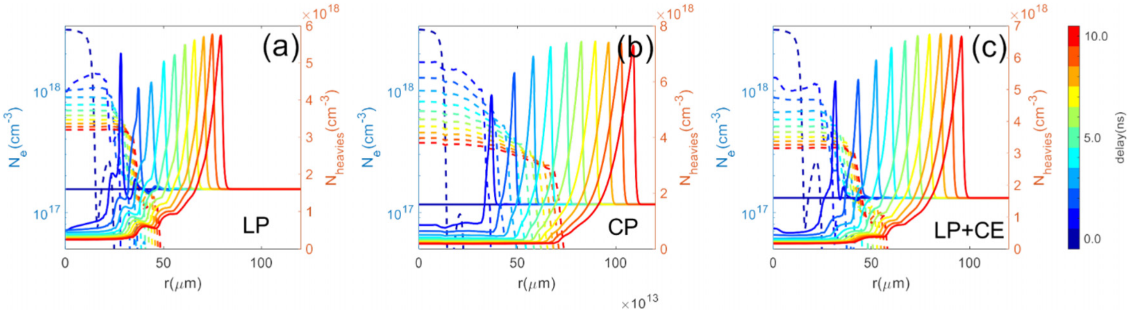

FIG. 3. Results from SPARC hydrodynamic simulation using initial conditions from YAPPE output for (a) LP and (b) CP. (c) LP + Coulomb explosion (CE) (linear polarization plus initial ion temperature $T_i = 3$ eV from Coulomb explosion).

2(b′)], by either the 2-Bessel method or self-waveguiding, forms the cladding. The LWFA results presented here use self-waveguiding: the radial wings in the far leading edge of the drive pulse ionizes the inside shock wall, generating a plasma waveguide cladding for the rest of the pulse.[7,18]

Accurate simulation of channel evolution is essential to accelerator design. Due to highly disparate timescales, simulations involve combining the results of two models, a hydrodynamic model for gas and plasma dynamics (nanosecond timescale) and a self-consistent femtosecond pulse propagation model to simulate Bessel beam-induced OFI of the gas and the effects of plasma-induced refractive distortion. Our recent work[20] comprehensively benchmarks OFI-based plasma waveguide generation and evolution using 2-color interferometry measurements plus the two models. Our propagation model [yet another pulse propagation effort (YAPPE)[18,20]] generates electron temperature and density profiles, which are input as initial conditions to the hydrodynamic code SPARC[62] to drive the evolution.

SPARC computes the evolution of the temperature, velocity, and density profiles of both combined ion/neutral heavy particles and electrons to model the hydrodynamic expansion, using rate equations that track H, H^+, $H_2{}^+$, and H_2 and its first two vibrational states.[20,62] Comparison of two-color interferometry measurements with simulations shows an interesting effect. In Figs. 2(a′) and 2(b′), waveguide expansion resulting from LP is similar to that from CP, even though CP induces significantly greater plasma heating (∼ 40 eV vs ∼ 10 eV for LP[20]). Further investigation suggested that LP pulses favor laser-

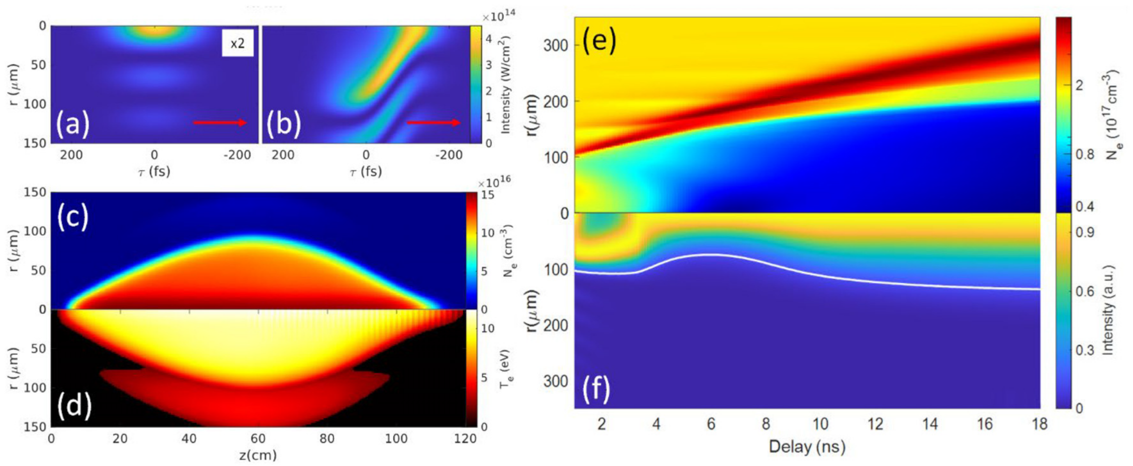

FIG. 4. Modeling of meter-length plasma waveguide using YAPPE and SPARC. (a) Intensity envelope of Bessel beam at $z = 4$ cm (intensity colormap has been multiplied $\times 2$). (b) Intensity envelope of Bessel beam at $z = 60$ cm. (c) Electron density profile at $\Delta t \sim 0^+$. (d) Electron temperature profile at $\Delta t \sim 0^+$, indicating a peak of $\sim$11 eV. (e) Plasma waveguide profile temporal evolution to $\Delta t = 18$ ns after OFI by the Bessel beam, calculated as the sum of the electron and neutral shock profiles, including ionization by self-waveguiding. (f) Fundamental quasi-bound mode intensity profile evolution, normalized at each delay. The mode's e^{-2} intensity radius is indicated by the white line. *Simulation parameters*: Temporal grid size 0.12 fs, temporal window size 500 fs, average radial grid size 2 μm, radial window size 1.6 cm, Bessel beam axis approach angle $\gamma = 10$ mrad, input beam radius 1 cm, and uniform hydrogen molecular density 1×10^{17} cm^{-3}.

induced Coulomb explosion (CE) of the hydrogen molecular ion $H_2^+ \rightarrow H^+ + H^+ + e$ because LP increases H_2^+ bond softening and ionization of intermediate vibrational states, directly producing protons with temperature ~ 3 eV.[20,63] This boost in ion temperature increases the expansion of the LP-generated channels (as seen in Fig. 3), accounting for the similar waveguide expansion from LP and CP beams seen in measurements in Fig. 2.

As an example of the full scope of YAPPE[18,20] and SPARC[62] modeling, Fig. 4 shows a Bessel beam-generated 1 m long plasma waveguide. The dramatic effect of distortion of the Bessel beam by plasma-induced refraction is seen by comparing the intensity envelopes earlier and later in the propagation. While the envelope is still relatively undistorted by $z = 4$ cm [Fig. 4(a)], it is highly distorted by $z = 60$ cm [Fig. 4(b)], where $N_e(r=0) \sim N_{cr}\sin^2\gamma = N_{cr,eff}$, the effective critical density. Figures 4(c) and 4(d) show the electron density and temperature profiles at $\Delta t = 0^+$ ns, immediately after Bessel beam passage. The resulting plasma pressure profile triggers hydrodynamic evolution computed by SPARC over $\Delta t = 0 - 18$ ns, where electron density profiles (assuming full ionization of the neutral shock by subsequent self-waveguiding) are shown in Fig. 4(e), with the corresponding fundamental quasi-bound mode[24] plotted in Fig. 4(f).

IV. RELATIVISTIC PULSE PROPAGATION IN METER-SCALE, LOW-DENSITY PLASMA WAVEGUIDES

To optimize electron charge and energy gain in multi-GeV LWFA, it is essential to understand the propagation of relativistic pulses (where $a_0 = eA_0/mc^2 \gtrsim 1$) in meter-scale low-density plasma waveguides. Here, a_0 is the peak normalized vector potential, A_0 is the vector potential, and e and m are the electron charge and mass. When relying on ionization injection, pulse evolution dictates the location and amount of charge injected into the wake. Pulse evolution also determines the strength of the wake's accelerating gradient, the electron beam spectrum, and dephasing between the laser pulse and the accelerated electron bunch. Our recent work[9] identifies three characteristic stages of relativistic pulse propagation in extended low-density plasma waveguides, including a new mode beating effect that occurs whether or not the pulse is linearly matched to the waveguide. This appears to be a universal effect in the propagation of high-intensity pulses in long, low-density plasma waveguides. This beating generates multi-peaked multi-GeV spectra due to periodic enhancement and suppression of ionization injection.

Figure 5 from Ref. 9 outlines the three-stage model as observed in 3D WarpX[64] particle-in-cell simulations with parameters similar to those in our experiments. Simulated channels were formed from 95% H_2/5% N_2 gas mix with hydrogen fully ionized and nitrogen ionized to N^{5+} corresponding to the channel structure shown in Fig. 5(d). The three stages are identified by labels I, II, and III alongside the blue curve in Fig. 5(a), which plots the evolution of a_0 for an initial pulse Gaussian in space and time ($a_{0i} = 2.0$, $\tau_{FWHM} = 41$ fs, $w_0 = 30\,\mu$m), mode-mismatched into a 20 cm long waveguide ($w_{ch} = 20\,\mu$m, $N_{e0} = 2.0 \times 10^{17}$ cm^{-3}). The waveguide transverse profile is plotted in Fig. 5(d).[9] Stage I describes large-amplitude oscillations in the early part of the waveguide from mode beating due to linear mode mismatch at laser injection. Since higher-order modes in the plasma waveguide propagate at a lower group velocity,[9,24] they increasingly lag behind and separate from the fundamental mode, leading to the decay of Stage I beating by $z \sim 3$ cm (see study of Ref. 9 for a detailed discussion).

Stage II is an extended, lower amplitude beating-induced oscillation that occurs whether or not the pulse is linearly mode matched to the waveguide, as one can see by comparing the blue and gold curves of Fig. 5(a). The gold curve plots the evolution of a_0 for the linearly mode-matched case. It lacks large stage I beating oscillations, yet it has axially extended stage II oscillations similar to the blue curve. The origin of these oscillations is ponderomotive modification of the

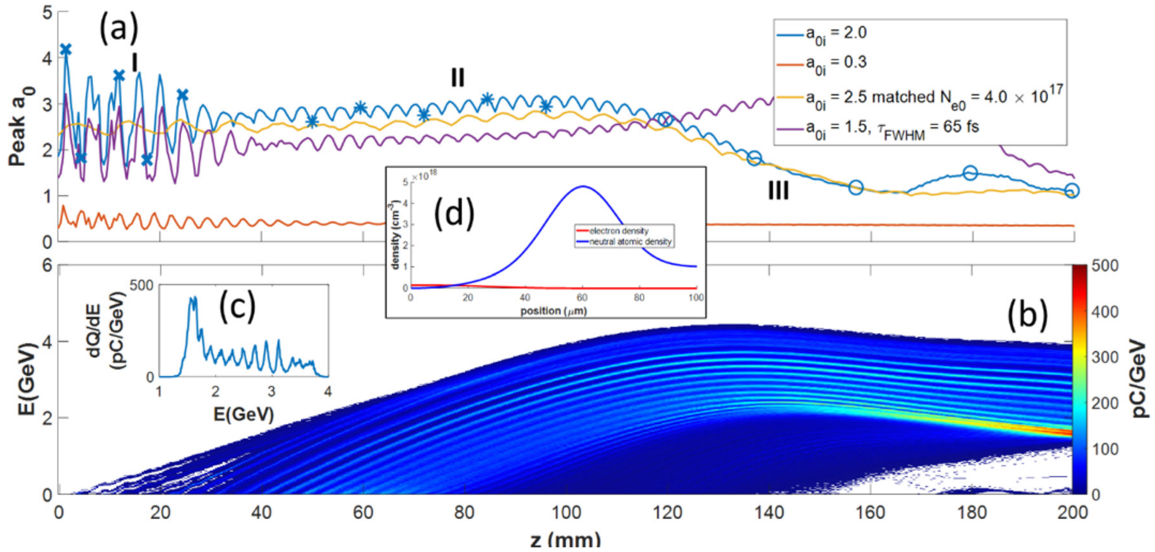

FIG. 5. Particle-in-cell WarpX[64] simulations of drive pulse evolution in a pre-ionized plasma waveguide. The simulation xyz grid is 256 × 256 × 4096 (256 × 256 × 204.8 μm^3) and gas composition is 95% H_2/5% N_2. (a) Peak laser field a_0 vs propagation distance for: blue curve—mismatched input field $a_{0i} = 2.0$, $w_0 = 30\,\mu m$, $\tau_{fwhm} = 41$ fs, $N_{e0} = 2.0 \times 10^{17}$ cm^{-3}, purple curve—mismatched input field $a_{0i} = 1.5$, $w_0 = 30\,\mu m$, $\tau_{fwhm} = 65$ fs, $N_{e0} = 2.0 \times 10^{17}$ cm^{-3}, and orange curve—mismatched $a_{0i} = 0.3$, $w_0 = 30\,\mu m$, $\tau_{fwhm} = 41$ fs, $N_{e0} = 2.0 \times 10^{17}$ cm^{-3}. The blue, purple, and orange curves all propagate in mismatched waveguide formed from the prepared index structure shown in (d), with $w_{ch} = 20\,\mu m$. Gold curve—matched Gaussian input $a_{0i} = 2.5$, $w_0 = 30\,\mu m$, $\tau_{fwhm} = 41$ fs propagating in parabolic channel with $w_{ch} = 30\,\mu m$, $N_{e0} = 4.0 \times 10^{17}$ cm^{-3}. Labels I, II, and III refer to the three characteristic propagation stages. (b) Electron spectrum vs propagation distance corresponding to the blue curve of (a). (c) Final integrated spectrum. (d) Prepared index structure measured by 2-color interferometry[18,20] and fitted to even polynomial × exponential.

waveguide's plasma density profile by the leading mode. As the pulse propagates, it continuously redshifts and couples energy into the fundamental $[(p, m) = (0, 0)]$ and first order radial mode $[(p, m) = (1, 0)]$ of the perturbed channel, where p and m are the radial and azimuthal mode indices. Stage II oscillations are caused by beating of the (0,0) and (1,0) modes in the perturbed channel, with period $\Lambda = 2\pi/|\beta_{10} - \beta_{00}| = \pi^2 \lambda_0 (w_{ch}/\lambda_0)^2$. The purple and blue curves in Fig. 5(a) both propagate through the same channel [shown in Fig. 5(d)], and therefore have the same beat period $\Lambda_{blue} = 4.0$ mm. The gold curve from Fig. 5(a) propagates through a matched parabolic $w_0 = w_{ch}^{gold} = 30\,\mu m$, which gives $\Lambda_{gold} = 7.1$ mm. As shown in Ref. 9, this simple beating model gives oscillation periods in quantitative agreement with those of the blue and gold curves.

Because of this continuous nonlinear energy coupling into the $(0, 0)$ and $(1, 0)$ modes, the beating amplitude remains relatively constant and occurs whether or not the drive pulse is linearly matched to the waveguide. The process thus appears to be universal. Only significantly reducing the pulse intensity (and therefore reducing channel modification) eliminates stage II beating, as shown by the orange curve in Fig. 5(a) depicting a mode-mismatched pulse injected with $a_{0i} = 0.3$, revealing that only stage I beating remains.[9] Stage II is followed by stage III, where the pulse disperses, stretches, redshifts, and a_0 declines.

The three stages of pulse propagation map directly to the enhancement and suppression of ionization injection, as seen in Fig. 5(b), which exhibits the integrated electron spectrum corresponding to the blue curve in Fig. 5(a). The large-amplitude oscillations in stage I cause wake distortion, only allowing a small amount of charge to be injected depending on idiosyncratic coupling dynamics. Instead, most of the charge is injected during stage II.

To further understand the enhancement and suppression of ionization injection, Fig. 6 from Ref. 9 compares the location of the injected charge with respect to (1) the oscillation peaks in a_0, (2) $\Delta\xi_{wake} = \xi_{wake} - \langle \xi_{wake} \rangle_{1\,\mathrm{cm}}$, the relative position of the back of the wake (the location where $E_z = 0$) in the moving simulation window, and (3) $\Delta\xi_{a_0,\,peak} = \xi_{a_0,\,peak} - \langle \xi_{a_0,\,peak} \rangle_{1\,\mathrm{cm}}$, the relative position of peak a_0 in the simulation window. Here, $\langle\,\rangle_{1\,\mathrm{cm}}$ denotes an average over 1 cm of propagation. It is clear from Fig. 6(a) that injection occurs mainly in stage II; stage I beating ($z <\sim 30$ mm) results in large oscillations in $\Delta\xi_{wake}$ that suppress electron injection, trapping, and acceleration.[9]

The injection peaks in stage II (marked by vertical dashed lines) occur at local oscillation minima of a_0, as seen in the green curve of Fig. 6(b). These minima correspond to locations where $\Delta\xi_{a_0,\,peak}$ suddenly changes sign [red curve in Fig. 6(b)], showing that ionization injection is enhanced when stage II beating moves the position of peak a_0 closest to the trapping center (location of $E_z = 0$ at the back of the wake) and suppressed when peak a_0 is moved furthest from the trapping center.[9] Note that $\Delta\xi_{wake}$ is an order of magnitude smaller than $\Delta\xi_{a_0,\,peak}$ in stage II, suggesting that back-and-forth oscillation of the wake (or oscillation of the wake velocity) is not the source of periodic enhancement and suppression of injection as may occur in other conditions.[66,67]

The three-stage model agrees well with plasma waveguide-based LWFA experiments conducted at the Laboratory for Advanced Lasers and Extreme Photonics[68] at Colorado State University. Details of the experiment can be found in Refs. 7–9 along with diagrams of the experimental setup. The general configuration is that the drive beam is focused into the end of the gas jet by an $f/25$ off-axis paraboloid, with

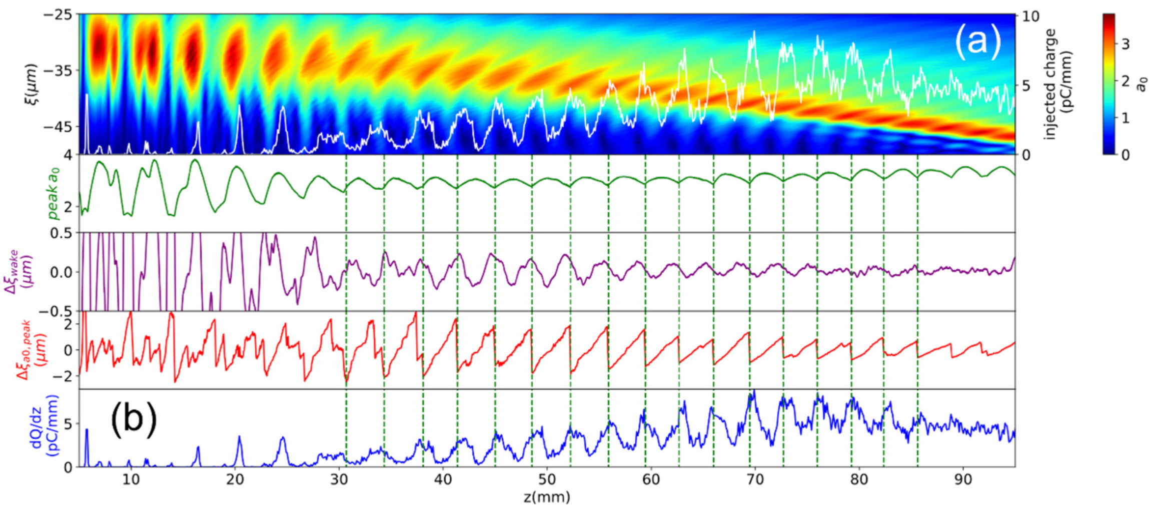

FIG. 6. Simulation with FBPIC[65] particle tracking, with parameters matching the blue curve of Fig. 5(a). (a) Evolution of the laser envelope (a_0) on-axis in the light frame (computation window, $\xi = z - v_g t$), showing the oscillations of the laser pulse peak and pulse retreat in the light frame. The white curve is a histogram of trapped electron injection locations with energy >50 MeV at $z = 10$ cm. (b) Lineouts of pulse and wake parameters vs propagation distance (see the text). Green curve: peak a_0 in moving window. Purple curve: relative position of the back of the wake, $\Delta\xi_{wake} = \xi_{wake} - \langle\xi_{wake}\rangle_{1\,\mathrm{cm}}$. Red curve: relative position of peak a_0, $\Delta\xi_{a_0,peak} = \xi_{a_0,peak} - \langle\xi_{a_0,peak}\rangle_{1\,\mathrm{cm}}$. Here, $\langle\,\rangle_{1\,\mathrm{cm}}$ refers to an average over 1 cm of propagation. Blue curve: replot of the white curve from panel (a).

the beam passing through a hole in a 45° mirror. The distance between the focal plane of the drive beam and the beginning of the jet was adjusted by moving the jet axially. A separate beam with a controllable pre-delay with respect to the drive beam was passed through a diffractive axicon; the beam was then reflected off the 45° mirror to form a Bessel beam in the gas jet and ionize it via OFI.

One notable demonstration was limiting injection to only one event by localizing the N_2 dopant to less than a stage II oscillation period at $z = 10$ cm or $z = 14$ cm, as shown in Fig. 7(b). The University of Maryland Gen. VI jet can localize the N_2 dopant to a ∼2.5 cm region, approximately the longitudinal period of stage II beating.

Initially, the 20 cm jet was doped along its full length using a 95% H_2/5% N_2 gas mix. Figure 7(a) shows multi-peaked, multi-GeV spectra, in qualitative agreement with the simulations of Figs. 5 and 6. Injection of the gas mix was then localized to an ∼2.5 cm longitudinal section centered either at $z = 10$ cm or $z = 14$ cm. Figure 7(b) shows mostly single-peaked multi-GeV spectra, with results for the injector at $z = 10$ cm to the left of the vertical white dashed line and results for $z = 14$ cm to the right of the vertical dashed line. These quasi-monoenergetic electron spectra have energy spreads < 10% and are a direct result of limiting the number of electron injection events from stage II oscillations via dopant gas restriction.[9]

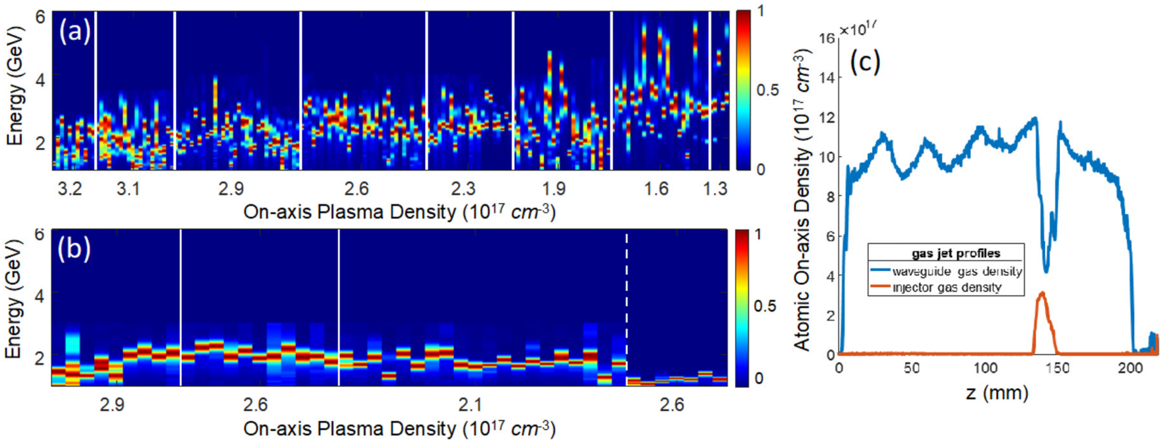

FIG. 7. Experimental data from[9] exhibiting angle-integrated (a) multi-peaked multi-GeV spectra when a whole 20 cm Gen. VI jet contained 95% H_2 5% N_2 gas mix and (b) single-peaked multi-GeV spectra when 20 cm Gen. VI jet was globally backed with pure H_2, except for a 2.5 cm region backed with 95% H_2 5% N_2 gas mix located at z = 10 cm (left of white dashed line) or z = 14 cm (right of white dashed line). Colormaps are normalized to the peak of each individual spectra. (c) Atomic gas density profile showing 2.5 cm localized injection section.

An additional experiment[9] employed a localized pure N_2 injection at $z = 14\,\text{cm}$. The jet's longitudinal gas density profile with the localized N_2 dopant is plotted in Fig. 7(c). Due to the slower hydrodynamic expansion of nitrogen plasma channels compared to hydrogen, this produced a localized region of the waveguide with a smaller fundamental mode. Results suggest that the sudden reduction in mode size increased the guided mode intensity, giving continuous ionization injection. This suggests that axially localized control of a waveguide mode structure may be harnessed to control injection into guided LWFAs.

V. HIGH EFFICIENCY LWFA WITH NANOCOULOMBS OF CHARGE IN THE 1–10 GeV RANGE

Further increasing the electron bunch energy and charge requires (1) improved efficiency of injected drive pulse coupling into the plasma waveguide, (2) injection of electrons earlier in propagation, and (3) optimized acceleration distance approaching but not surpassing the dephasing length. Results from our recent work benchmarking plasma waveguides[20] enabled us to finely tune the waveguide fundamental mode radius w_{ch} to match the drive beam waist radius w_0 ($\approx 30\,\mu\text{m}$ at low power). Rather than using a delay line to adjust w_{ch} via the timing of the waveguide forming Bessel beam in advance of the injected drive pulse,[7,9] the delay was fixed, and the Bessel beam energy was adjusted using a half-waveplate and thin film polarizer, enabling continuous control of w_{ch}. Here, we used a 4-level diffractive axicon to generate the Bessel beam, which had a ray axis approach angle of 2.3°.

To increase electron energy gain and extend the dephasing length to $\sim 30\,\text{cm}$, the on-axis plasma density was reduced to $N_{e0} \sim 1.3 \times 10^{17}\,\text{cm}^{-3}$, and the Bessel beam energy was scanned to mode match the waveguide to the drive pulse, minimizing stage I mode beating and wake distortion. To reach lower N_{e0}, 1% N_2 dopant was used rather than 5%. In addition, the drive pulse duration was adjusted by scanning the compressor grating spacing. These optimizations ($\sim 18\,\text{J}$ pulse with $\tau_{FWHM} \approx 60\,\text{fs}$) enabled injection and trapping of $\sim 10\,\text{pC}$ early in propagation and accelerated above 9 GeV with spectral features extending beyond 10 GeV.

The 50 highest energy electron spectra are displayed in Fig. 8, plotted on a log colormap to reveal comparatively lower-charge spectral features. The spectra in panel (a) are angle-resolved, and those in panel (b) are angle-integrated. Note that the log scale exaggerates the angular width of the spectra in panel (a), which mostly are of sub-milliradian divergence when plotted on a linear colormap. The highest energy features/tails contain $\sim 10\,\text{pC}$ above $\sim 9\,\text{GeV}$ and extend beyond 10 GeV. FBPIC[65] simulations suggest that the high-energy features are injected during stage I beating and the high charge, multi-peaked portions of the spectra are injected during stage II.[9] Since the full 30 cm jet was doped with 1% N_2, stage II mode beating injected more charge overall, accelerating >1 nC of measured charge (passing through the electron spectrometer collimating slit) to energies >1 GeV. The directly measured conversion efficiency of laser-to-electron energy >1 GeV was 30%, calculated by integrating the electron spectra over angular distribution, energy, and charge, and then compared to the on-target drive beam energy. Because the electron beam generally significantly overfills the slit (see below), the actual conversion efficiency[46] is at least 30%.

Drive beam pointing instability[7] causes fluctuations in coupling efficiency, bound mode content, and wakefield dynamics, resulting in shot-to-shot variation of electron beam spectra (as seen in Fig. 8 and in Refs. 7 and 9) and beam alignment to the spectrometer entrance slit. The measured accelerated charge passing through the slit varied from

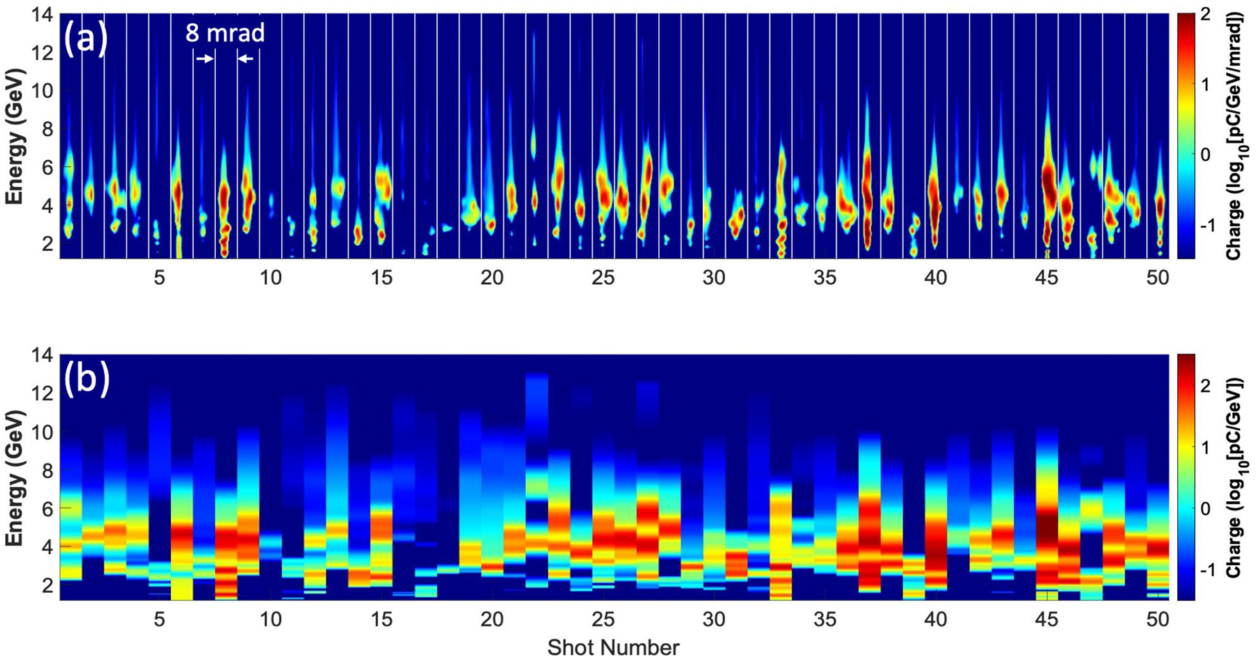

FIG. 8. (a) Angle-resolved electron bunch spectra plotted on log colormap for 50 high-energy shots; angular range for each spectral strip is 8 mrad. (b) Angle-integrated version of (a). Charge measurements are for the beam that has passed through the slit. Highest energy features/tails include ~10 pC and extend beyond 10 GeV.

200 pC to 1.4 nC in the 1–8 GeV range. The collimating slit consisted of 10 cm deep, 0.5 mm spaced tungsten blocks in advance of the magnetic spectrometer (see details in Ref. 7). Imaging the full electron beam profile on a LANEX screen before the spectrometer slit revealed that, on average, <50% of the electron beam entered the slit, implying that quoted charge and energy efficiency is underestimated by up to a factor of 2. We found that with the slit sampling different sections of the beam as its pointing varied, all sampled portions had multi-GeV spectra.

Our methods for generating hydrodynamic waveguides by Bessel beam ionization and heating of meter-scale gas jets are being employed at other institutions, leading to significant increases in electron beam efficiency and quality. Recent experiments[15] at Lawrence Berkeley National Laboratory (LBNL) in collaboration with the University of Maryland employed this approach with a 21.3 J drive laser (∼500 TW) and a 30 cm gas jet to demonstrate acceleration of 6 pC electron bunches in an isolated quasi-monoenergetic peak at ∼9.2 GeV. In this case, the dopant was intentionally restricted to the first ∼12 cm, increasing gain and limiting the injection during stage II. This result is to be compared to prior LBNL work[13] in which a discharge capillary plasma waveguide required 800 TW drive pulses to accelerate 5 pC to 7.8 GeV in a spectral tail. This highlights the reproducibility and efficacy of the experimental methods we have pioneered.

VI. METER-LENGTH GAS JET DEVELOPMENT FOR ELECTRON ACCELERATION BEYOND 10 GeV

Pushing high-energy LWFA beyond 10 GeV requires extending propagation in low-density plasma waveguides to lengths ∼1 m. For longer acceleration lengths, a modular jet design is preferable because it achieves fabrication tolerances more easily over extended lengths, enables extension to lengths limited only by the increasing gas load in vacuum systems, and provides axial control of gas density and composition. One application is a density up-ramp for re-phasing accelerated electron bunches with the plasma wake, boosting electron energy gain.[69–71] For LWFA acceleration to tens of GeV in meter-scale distances, density up ramps are required.[72] Jets with custom density profiles can also be used for localized gas dopant to control ionization injection,[72–74] down ramp injection,[75,76] long wavelength infrared generation,[77,78] betatron generation,[79] and staging.[10,80]

In a continuation of its gas jet development program, the Intense Laser Matter Interactions Lab at the University of Maryland recently developed and characterized the first modular meter-scale supersonic (Gen. VII) gas jet, well suited to all of these applications.[19] The Mach 5 Gen. VII jet is constructed from 11 cm long modules and is extendable to any length. A diagram of two attached modules is shown in Fig. 9(a). Each module is divided into three sections, each of which is fed by a single solenoid valve. The valves have a common gas supply manifold, which is also modular. Each module has additional gas input ports for dopant injection, for example, enabling complete control of gas composition and/or density. To test engineering feasibility, a 1.0 m long jet was assebled with nine modules (27 sections) and spacers and backed with pure hydrogen (except for one section backed with N_2). A 1 m long Bessel beam-generated plasma was formed over the jet backed with 6.9 bars (100 psi) of pure hydrogen, shown in Fig. 9(b), an image of hydrogen recombination fluorescence taken through an H–α line filter. To our knowledge, this is the longest gas jet laser-plasma yet generated. The 3.4 cm long section backed with pure N_2, therefore, appears as dark. A more detailed discussion can be found in Ref. 19.

The density of each gas section can be controlled with solenoid valve timing (transient control) or valve flow rates (steady state control). We have characterized the jet with transient control, where all valves share a power supply but have independent trigger delays. This provides significant flexibility for controlling gas density in each section. Figure 10(a) plots colourmaps of the axially resolved H_2 gas density 1.2 cm above the jet orifice as a function of delay after valve triggering at $t = 0$, measured using our fluorescence technique.[7,8] Earlier than ∼3 ms, there is negligible fluorescence signal, and the signal reaches steady state at

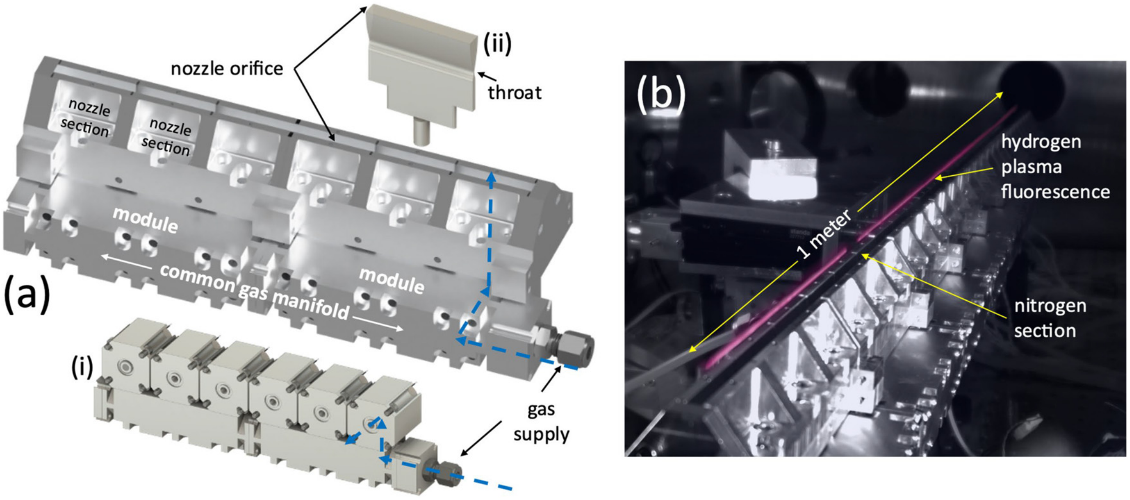

FIG. 9. (a) 3D model of a two-module supersonic gas jet, comprised of manifolds, nozzles, and valves (behind the manifolds). Gas flow directions in the manifold and the nozzle are indicated with dashed arrows. (i) Model of the manifold showing valve couplers. (ii) Internal flow volume showing orifice and throat positions. (b) A 1 m long hydrogen plasma florescence generated using modular supersonic gas jet backed with 6.9 bars (100 psi) in use in vacuum. One of the 27 sections is backed with nitrogen. The plasma is generated with a pulse (800 mJ, ∼ 75 fs) focused by a diffractive logarithmic axicon[33] and fluorescence is captured with an H–α line filter where the nitrogen section is shown as a gap.

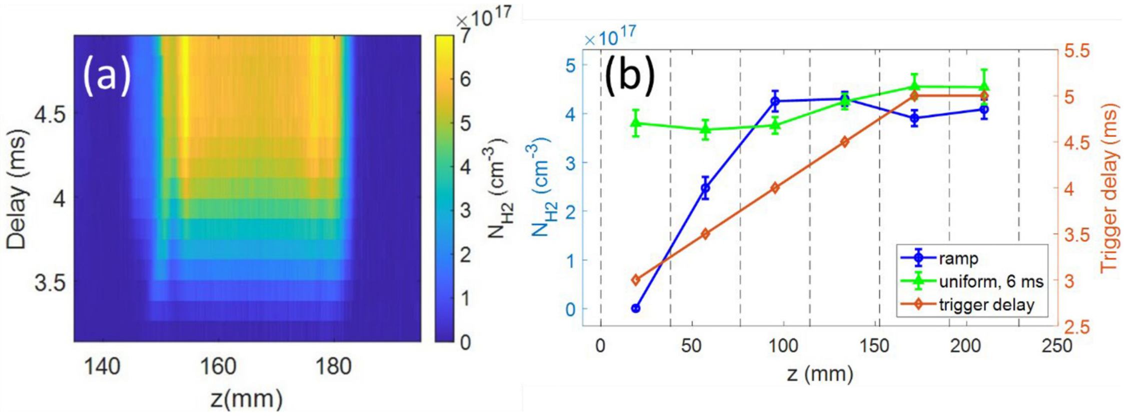

FIG. 10. (a) Temporal evolution of H_2 density taken $h = 8$ mm above single nozzle section. At each delay, the density is averaged over 10 shots. Each valve is driven by a 48VDC, 5 ms square wave pulse, and backed by 5.5 bars (80 psi). (b) Demonstration of control over axial density profile using 2 modules (6 nozzle sections) by altering valve timing. The fluorescence method[7,8] is used to measure the H_2 axial density profile. For the green curve, all valves are triggered with a 6 ms delay. For the blue curve, the valve trigger delays are (from left to right) 3, 3.5, 4, 4.5, 5, and 5 ms (delays are also plotted on the red curve). Each point represents a 10-shot average of the mean density across the center 1 cm window of each nozzle section. The nozzle section boundaries are marked by dashed lines.

$\sim$4.5 ms. The transition to steady state takes $\sim$1 ms with a nearly linear temporal ramp. Thus, a custom density profile can be built by appropriately adjusting the trigger time of each valve.

Figure 10(b) plots an example axial gas density profile along with the accompanying valve trigger delays for a two-module jet (6 sections), where each point represents a 10-shot average density of the middle 1 cm region of each section. The baseline profile (green curve) obtained for the valves triggered at the same delay (6 ms) is compared to a ramped/flat profile generated by staggered triggering (blue curve). The red curve plots the valve delays used.

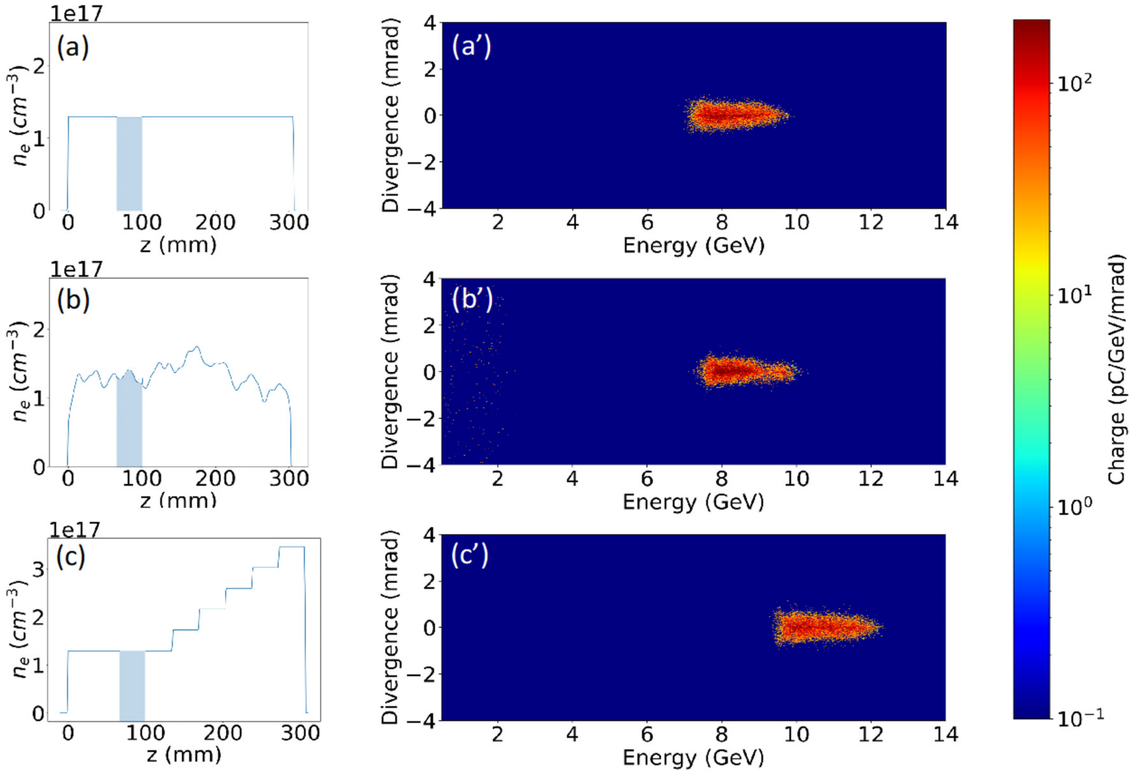

FIG. 11. Density profiles with resulting electron spectra from channel guided LWFA in (a) uniform channel, (b) measured density profile of the Gen. VI jet, and (c) density up ramp. (a')–(c') Final angle-resolved electron spectra corresponding to (a)–(c).

To explore the capabilities of a 30 cm long modular jet, we ran FBPIC[65] simulations with three different density profiles shown in Fig. 11: (a) flat, (b) measured profile of the Gen VI gas jet, and (c) a staircase up ramp. Nitrogen dopant for ionization injection (1% by number density) was located in the interval $z = 6.7 - 10$ cm. In each simulation, a laser pulse ($\tau_{FWHM} = 55$ fs, $\lambda = 800$ nm, $w_0 =$ 30 μm $a_{0i} = 3.2$) was mode matched into the waveguide, assumed to have a parabolic density profile. Angularly resolved accelerated electron bunch spectra from these axial profiles are shown in Figs. 11(a')–11(c'). Spectra from the profiles of (a) and (b) are similar in energy and divergence. The spectrum in Fig. 11(c') shows a clear boost in electron beam energy, from ∼8.5 to ∼11 GeV. The density profile of Fig. 11(c) is achievable with our modular Gen. VII gas jet and shows clear promise for future LWFA experiments. Recent simulations[72] employing a 312.3 J laser pulse ($\tau_0 = 212$ fs, $r_0 = 84.9$ μm) demonstrate production of 100 GeV electron bunches in a single, 6 m LWFA stage employing a linear density up-ramp.

VII. CONCLUSIONS

The development of long supersonic gas jets and optical techniques for generating meter-scale plasma waveguides[17–20] at the University of Maryland has opened the door to a new generation of multi-GeV laser wakefield accelerators.[7–9,15] Since these initial experiments, LWFA electron beam quality and energy have rapidly improved due to our supersonic gas jet development,[19] comprehensive benchmarking of the generation and evolution of OFI plasma waveguides,[20] and modeling of relativistic pulse evolution in these waveguides.[7,9] Collectively, these developments have facilitated the most consistent and efficient production of multi-GeV LWFA electron bunches to date, including ∼50 shots with at least nC-level charge above 1 GeV, sub-milliradian beam divergence, and electron bunches accelerated to ∼10 GeV and slightly beyond, achieving laser-to-electron beam energy efficiency of at least 30%.[46] Our recent development of a modular supersonic gas jet[19] enables multi-meter plasma waveguides with customizable axial profiles, laying a path toward significantly increased acceleration length, bunch energy, and beam quality.

ACKNOWLEDGMENTS

The authors thank Mayank Gupta, Nishchal Tripathi, Frederica Sorkin, Alex Picksley, Josh Stackhouse, and Sebastian Lorenz for lab assistance and/or technical discussions. This work was supported by the U.S. Department of Energy (DE-SC0015516, LaserNetUS DE-SC0019076/ FWP#SCW1668, and DE-SC0011375), and the Defense Advanced Research Projects Agency (DARPA) under the Muons for Science and Security Program. E. Rockafellow was supported by NSF GRFP (Grant No. DGE 1840340).

AUTHOR DECLARATIONS

Conflict of Interest

The authors have no conflicts to disclose.

Author Contributions

E. Rockafellow: Conceptualization (equal); Data curation (equal); Formal analysis (equal); Investigation (equal); Methodology (equal); Software (equal); Supervision (equal); Validation (equal); Visualization (equal); Writing – original draft (equal); Writing – review & editing (equal). **B. Miao:** Conceptualization (equal); Data curation (equal); Formal analysis (equal); Investigation (equal); Methodology (equal); Software (equal); Supervision (equal); Validation (equal); Visualization (equal); Writing – original draft (equal); Writing – review & editing (equal). **J. E. Shrock:** Conceptualization (equal); Data curation (equal); Formal analysis (equal); Investigation (equal); Methodology (equal); Software (equal); Supervision (equal); Validation (equal); Visualization (equal); Writing – original draft (equal); Writing – review & editing (equal). **A. Sloss:** Conceptualization (equal); Data curation (equal); Formal analysis (equal); Investigation (equal); Methodology (equal); Software (equal); Validation (equal); Visualization (equal); Writing – review & editing (equal). **M. S. Le:** Investigation (supporting); Software (supporting); Visualization (supporting). **S. W. Hancock:** Investigation (supporting); Methodology (supporting); Software (supporting). **S. Zahedpour:** Investigation (supporting); Methodology (supporting); Resources (supporting). **R. C. Hollinger:** Investigation (supporting); Methodology (supporting); Resources (supporting). **S. Wang:** Investigation (supporting); Methodology (supporting); Resources (supporting). **J. King:** Investigation (supporting). **P. Zhang:** Investigation (supporting). **J. Šišma:** Investigation (supporting). **G. M. Grittani:** Investigation (supporting). **R. Versaci:** Investigation (supporting). **D. F. Gordon:** Investigation (supporting); Software (supporting). **G. J. Williams:** Investigation (supporting); Methodology (supporting); Resources (supporting). **B. A. Reagan:** Investigation (supporting); Methodology (supporting); Project administration (supporting); Resources (supporting). **J. J. Rocca:** Investigation (supporting); Methodology (supporting); Resources (supporting). **H. M. Milchberg:** Conceptualization (equal); Data curation (equal); Formal analysis (equal); Funding acquisition (equal); Investigation (equal); Methodology (equal); Project administration (equal); Resources (equal); Software (equal); Supervision (equal); Validation (equal); Visualization (equal); Writing – original draft (equal); Writing – review & editing (equal).

DATA AVAILABILITY

The data that support the findings of this study are available within the article and also from the corresponding author upon reasonable request.

REFERENCES

[1] N. D. Powers, I. Ghebregziabher, G. Golovin, C. Liu, S. Chen, S. Banerjee, J. Zhang, and D. P. Umstadter, "Quasi-monoenergetic and tunable X-rays from a laser-driven Compton light source," Nat. Photonics **8**, 28–31 (2014).
[2] F. Albert and A. G. R. Thomas, "Applications of laser wakefield accelerator-based light sources," Plasma Phys. Controlled Fusion **58**(10), 103001 (2016).
[3] W. Wang, K. Feng, L. Ke, C. Yu, Y. Xu, R. Qi, Y. Chen, Z. Qin, Z. Zhang, M. Fang, J. Liu, K. Jiang, H. Wang, C. Wang, X. Yang, F. Wu, Y. Leng, J. Liu, R. Li, and Z. Xu, "Free-electron lasing at 27 nanometres based on a laser wakefield accelerator," Nature **595**, 516–520 (2021).
[4] C. B. Schroeder, E. Esarey, C. G. R. Geddes, C. Benedetti, and W. P. Leemans, "Physics considerations for laser-plasma linear colliders," Phys. Rev. Spec. Top.–Accel. Beams **13**(10), 101301 (2010).
[5] E. Esarey, C. B. Schroeder, and W. P. Leemans, "Physics of laser-driven plasma-based electron accelerators," Rev. Mod. Phys. **81**(3), 1229–1285 (2009).
[6] E. Esarey, P. Sprangle, J. Krall, and A. Ting, "Overview of plasma-based accelerator concepts," IEEE Trans. Plasma Sci. **24**(2), 252–288 (1996).
[7] B. Miao, J. E. Shrock, L. Feder, R. C. Hollinger, J. Morrison, R. Nedbailo, A. Picksley, H. Song, S. Wang, J. J. Rocca, and H. M. Milchberg, "Multi-GeV electron bunches from an all-optical laser wakefield accelerator," Phys. Rev. X **12**(3), 031038 (2022).

[8] J. E. Shrock, B. Miao, L. Feder, and H. M. Milchberg, "Meter-scale plasma waveguides for multi-GeV laser wakefield acceleration," Phys. Plasmas **29**(7), 073101 (2022).

[9] J. E. Shrock, E. Rockafellow, B. Miao, M. Le, R. C. Hollinger, S. Wang, A. J. Gonsalves, A. Picksley, J. J. Rocca, and H. M. Milchberg, "Guided mode evolution and ionization injection in meter-scale multi-GeV laser wakefield accelerators," Phys. Rev. Lett. **133**(4), 045002 (2024).

[10] H. T. Kim, K. H. Pae, H. J. Cha, I. J. Kim, T. J. Yu, J. H. Sung, S. K. Lee, T. M. Jeong, and J. Lee, "Enhancement of electron energy to the multi-GeV regime by a dual-stage laser-wakefield accelerator pumped by petawatt laser pulses," Phys. Rev. Lett. **111**(16), 165002 (2013).

[11] X. Wang, R. Zgadzaj, N. Fazel, Z. Li, S. A. Yi, X. Zhang, W. Henderson, Y.-Y. Chang, R. Korzekwa, H.-E. Tsai, C.-H. Pai, H. Quevedo, G. Dyer, E. Gaul, M. Martinez, A. C. Bernstein, T. Borger, M. Spinks, M. Donovan, V. Khudik, G. Shvets, T. Ditmire, and M. C. Downer, "Quasi-monoenergetic laser-plasma acceleration of electrons to 2 GeV," Nat. Commun. **4**, 1988 (2013).

[12] W. P. Leemans, A. J. Gonsalves, H.-S. Mao, K. Nakamura, C. Benedetti, C. B. Schroeder, C. Tóth, J. Daniels, D. E. Mittelberger, S. S. Bulanov, J.-L. Vay, C. G. R. Geddes, and E. Esarey, "Multi-GeV electron neams from capillary-discharge-guided subpetawatt laser pulses in the self-trapping regime," Phys. Rev. Lett. **113**(24), 245002 (2014).

[13] A. J. Gonsalves, K. Nakamura, J. Daniels, C. Benedetti, C. Pieronek, T. C. H. de Raadt, S. Steinke, J. H. Bin, S. S. Bulanov, J. van Tilborg, C. G. R. Geddes, C. B. Schroeder, C. Tóth, E. Esarey, K. Swanson, L. Fan-Chiang, G. Bagdasarov, N. Bobrova, V. Gasilov, G. Korn, P. Sasorov, and W. P. Leemans, "Petawatt laser guiding and electron beam acceleration to 8 GeV in a laser-heated capillary discharge waveguide," Phys. Rev. Lett. **122**(8), 084801 (2019).

[14] C. Aniculaesei, T. Ha, S. Yoffe, L. Labun, S. Milton, E. McCary, M. M. Spinks, H. J. Quevedo, O. Z. Labun, R. Sain, A. Hannasch, R. Zgadzaj, I. Pagano, J. A. Franco-Altamirano, M. L. Ringuette, E. Gaul, S. V. Luedtke, G. Tiwari, B. Ersfeld, E. Brunetti, H. Ruhl, T. Ditmire, S. Bruce, M. E. Donovan, M. C. Downer, D. A. Jaroszynski, and B. M. Hegelich, "The acceleration of a high-charge electron bunch to 10 GeV in a 10-cm nanoparticle-assisted wakefield accelerator," Matter Radiat. Extremes **9**(1), 014001 (2024).

[15] A. Picksley, J. Stackhouse, C. Benedetti, K. Nakamura, H. E. Tsai, R. Li, B. Miao, J. E. Shrock, E. Rockafellow, H. M. Milchberg, C. B. Schroeder, J. van Tilborg, E. Esarey, C. G. R. Geddes, and A. J. Gonsalves, "Matched guiding and controlled injection in dark-current-free, 10-GeV-class, channel-guided laser-plasma accelerators," Phys. Rev. Lett. **133**(25), 255001 (2024).

[16] W. Lu, M. Tzoufras, C. Joshi, F. S. Tsung, W. B. Mori, J. Vieira, R. A. Fonseca, and L. O. Silva, "Generating multi-GeV electron bunches using single stage laser wakefield acceleration in a 3D nonlinear regime," Phys. Rev. Spec. Top.–Accel. Beams **10**(6), 061301 (2007).

[17] B. Miao, L. Feder, J. E. Shrock, A. Goffin, and H. M. Milchberg, "Optical guiding in meter-scale plasma waveguides," Phys. Rev. Lett. **125**(7), 074801 (2020).

[18] L. Feder, B. Miao, J. E. Shrock, A. Goffin, and H. M. Milchberg, "Self-waveguiding of relativistic laser pulses in neutral gas channels," Phys. Rev. Res. **2**(4), 043173 (2020).

[19] B. Miao, J. E. Shrock, E. Rockafellow, A. J. Sloss, and H. M. Milchberg, "Meter-scale supersonic gas jets for multi-GeV laser-plasma accelerators," Rev. Sci. Instrum. **96**, 043003 (2025).

[20] B. Miao, E. Rockafellow, J. E. Shrock, S. W. Hancock, D. Gordon, and H. M. Milchberg, "Benchmarking of hydrodynamic plasma waveguides for multi-GeV laser-driven electron acceleration," Phys. Rev. Accel. Beams **27**(8), 081302 (2024).

[21] C. G. Durfee and H. M. Milchberg, "Light pipe for high intensity laser pulses," Phys. Rev. Lett. **71**(15), 2409–2412 (1993).

[22] C. G. Durfee, J. Lynch, and H. M. Milchberg, "Development of a plasma waveguide for high-intensity laser pulses," Phys. Rev. E **51**(3), 2368–2389 (1995).

[23] Y. Ehrlich, C. Cohen, A. Zigler, J. Krall, P. Sprangle, and E. Esarey, "Guiding of high intensity laser pulses in straight and curved plasma channel experiments," Phys. Rev. Lett. **77**(20), 4186–4189 (1996).

[24] T. R. Clark and H. M. Milchberg, "Optical mode structure of the plasma waveguide," Phys. Rev. E **61**(2), 1954–1965 (2000).

[25] A. Butler, D. J. Spence, and S. M. Hooker, "Guiding of high-intensity laser pulses with a hydrogen-filled capillary discharge waveguide," Phys. Rev. Lett. **89**(18), 185003 (2002).

[26] N. Lemos, T. Grismayer, L. Cardoso, G. Figueira, R. Issac, D. A. Jaroszynski, and J. M. Dias, "Plasma expansion into a waveguide created by a linearly polarized femtosecond laser pulse," Phys. Plasmas **20**(6), 063102 (2013).

[27] N. Lemos, L. Cardoso, J. Geada, G. Figueira, F. Albert, and J. M. Dias, "Guiding of laser pulses in plasma waveguides created by linearly-polarized femtosecond laser pulses," Sci. Rep. **8**, 3165 (2018).

[28] R. J. Shalloo, C. Arran, L. Corner, J. Holloway, J. Jonnerby, R. Walczak, H. M. Milchberg, and S. M. Hooker, "Hydrodynamic optical-field-ionized plasma channels," Phys. Rev. E **97**(5), 053203 (2018).

[29] S. Smartsev, C. Caizergues, K. Oubrerie, J. Gautier, J.-P. Goddet, A. Tafzi, K. Ta Phuoc, V. Malka, and C. Thaury, "Axiparabola: A long-focal-depth, high-resolution mirror for broadband high-intensity lasers," Opt. Lett. **44**(14), 3414 (2019).

[30] R. J. Shalloo, C. Arran, A. Picksley, A. von Boetticher, L. Corner, J. Holloway, G. Hine, J. Jonnerby, H. M. Milchberg, C. Thornton, R. Walczak, and S. M. Hooker, "Low-density hydrodynamic optical-field-ionized plasma channels generated with an axicon lens," Phys. Rev. Accel. Beams **22**(4), 041302 (2019).

[31] A. Picksley, A. Alejo, J. Cowley, N. Bourgeois, L. Corner, L. Feder, J. Holloway, H. Jones, J. Jonnerby, H. M. Milchberg, L. R. Reid, A. J. Ross, R. Walczak, and S. M. Hooker, "Guiding of high-intensity laser pulses in 100-mm-long hydrodynamic optical-field-ionized plasma channels," Phys. Rev. Accel. Beams **23**(8), 081303 (2020).

[32] A. Picksley, A. Alejo, R. J. Shalloo, C. Arran, A. von Boetticher, L. Corner, J. A. Holloway, J. Jonnerby, O. Jakobsson, C. Thornton, R. Walczak, and S. M. Hooker, "Meter-scale conditioned hydrodynamic optical-field-ionized plasma channels," Phys. Rev. E **102**(5), 053201 (2020).

[33] N. Tripathi, B. Miao, A. Sloss, E. Rockafellow, and J. Shrock, "Longitudinal shaping of plasma waveguides using diffractive axicons for laser wakefield acceleration," Opt. Lett. (to be published) (2025).

[34] T. R. Clark and H. M. Milchberg, "Frequency selective tunnel coupling to the plasma fiber," Phys. Rev. Lett. **81**(2), 357–360 (1998).

[35] C. G. Durfee, J. Lynch, and H. M. Milchberg, "Mode properties of a plasma waveguide for intense laser pulses," Opt. Lett. **19**(23), 1937–1939 (1994).

[36] T. R. Clark and H. M. Milchberg, "Time- and space-resolved density evolution of the plasma waveguide," Phys. Rev. Lett. **78**(12), 2373–2376 (1997).

[37] W. P. Leemans, B. Nagler, A. J. Gonsalves, C. Tóth, K. Nakamura, C. G. R. Geddes, E. Esarey, C. B. Schroeder, and S. M. Hooker, "GeV electron beams from a centimetre-scale accelerator," Nat. Phys. **2**(10), 696–699 (2006).

[38] A. Zigler, Y. Ehrlich, C. Cohen, J. Krall, and P. Sprangle, "Optical guiding of high-intensity laser pulses in a long plasma channel formed by a slow capillary discharge," J. Opt. Soc. Am. B **13**, 68–71 (1996).

[39] N. A. Bobrova, A. A. Esaulov, J.-I. Sakai, P. V. Sasorov, D. J. Spence, A. Butler, S. M. Hooker, and S. V. Bulanov, "Simulations of a hydrogen-filled capillary discharge waveguide," Phys. Rev. E **65**(1), 016407 (2001).

[40] S. Karsch, J. Osterhoff, A. Popp, T. P. Rowlands-Rees, Z. Major, M. Fuchs, B. Marx, R. Hörlein, K. Schmid, L. Veisz, S. Becker, U. Schramm, B. Hidding, G. Pretzler, D. Habs, F. Grüner, F. Krausz, and S. M. Hooker, "GeV-scale electron acceleration in a gas-filled capillary discharge waveguide," New J. Phys. **9**(11), 415 (2007).

[41] T. P. Rowlands-Rees, C. Kamperidis, S. Kneip, A. J. Gonsalves, S. P. D. Mangles, J. G. Gallacher, E. Brunetti, T. Ibbotson, C. D. Murphy, P. S. Foster, M. J. V. Streeter, F. Budde, P. A. Norreys, D. A. Jaroszynski, K. Krushelnick, Z. Najmudin, and S. M. Hooker, "Laser-driven acceleration of electrons in a partially ionized plasma channel," Phys. Rev. Lett. **100**(10), 105005 (2008).

[42] A. J. Gonsalves, K. Nakamura, C. Benedetti, C. V. Pieronek, S. Steinke, J. H. Bin, S. S. Bulanov, J. van Tilborg, C. G. R. Geddes, C. B. Schroeder, J. Daniels, C. Tóth, L. Obst-Huebl, R. G. W. van den Berg, G. Bagdasarov, N. Bobrova, V. Gasilov, G. Korn, P. Sasorov, W. P. Leemans, and E. Esarey, "Laser-heated capillary discharge plasma waveguides for electron acceleration to 8 GeV," Phys. Plasmas **27**(5), 053102 (2020).

[43] A. Picksley, J. Chappell, E. Archer, N. Bourgeois, J. Cowley, D. R. Emerson, L. Feder, X. J. Gu, O. Jakobsson, A. J. Ross, W. Wang, R. Walczak, and S. M. Hooker, "All-optical GeV electron bunch generation in a laser-plasma accelerator via truncated-channel injection," Phys. Rev. Lett. **131**(24), 245001 (2023).

[44] A. Morozov, A. Goltsov, Q. Chen, M. Scully, and S. Suckewer, "Ionization assisted self-guiding of femtosecond laser pulses," Phys. Plasmas **25**(5), 053110 (2018).

[45] B. Miao, L. Feder, J. E. Shrock, and H. M. Milchberg, "Phase front retrieval and correction of Bessel beams," Opt. Express **30**(7), 11360–11371 (2022).

[46] J. E. Shrock, E. Rockafellow, B. Miao, A. Sloss, S. Wang, S. Zahedpur, R. C. Hollinger, J. Sisma, G. Grittani, J. Stackhouse, A. J. Gonsalves, J. Williams, B. Reagan, J. J. Rocca, and H. M. Milchberg, "Efficient production of multi-Joule, multi-GeV electron beams in a tunable all optical laser wakefield accelerator," (unpublished).

[47] T. L. Audet, P. Lee, G. Maynard, S. D. Dufrénoy, A. Maitrallain, M. Bougeard, P. Monot, and B. Cros, "Gas cell density characterization for laser wakefield acceleration," Nucl. Instrum. Methods Phys. Res., Sect. A **909**, 383–386 (2018).

[48] J. Osterhoff, A. Popp, Z. Major, B. Marx, T. P. Rowlands-Rees, M. Fuchs, M. Geissler, R. Hörlein, B. Hidding, S. Becker, E. A. Peralta, U. Schramm, F. Grüner, D. Habs, F. Krausz, S. M. Hooker, and S. Karsch, "Generation of stable, low-divergence electron beams by laser-wakefield acceleration in a steady-state-flow gas cell," Phys. Rev. Lett. **101**(8), 085002 (2008).

[49] J. Kim, V. L. J. Phung, K. Roh, M. Kim, K. Kang, and H. Suk, "Development of a density-tapered capillary gas cell for laser wakefield acceleration," Rev. Sci. Instrum. **92**(2), 023511 (2021).

[50] S. P. Nikitin, I. Alexeev, J. Fan, and H. M. Milchberg, "High efficiency coupling and guiding of intense femtosecond laser pulses in preformed plasma channels in an elongated gas jet," Phys. Rev. E **59**(4), R3839–R3842 (1999).

[51] B. D. Layer, A. York, T. M. Antonsen, S. Varma, Y.-H. Chen, Y. Leng, and H. M. Milchberg, "Ultrahigh-intensity optical slow-wave structure," Phys. Rev. Lett. **99**(3), 035001 (2007).

[52] G. A. Hine, A. J. Goers, L. Feder, J. A. Elle, S. J. Yoon, and H. M. Milchberg, "Generation of axially modulated plasma waveguides using a spatial light modulator," Opt. Lett. **41**(15), 3427–3430 (2016).

[53] H. Sheng, K. Y. Kim, V. Kumarappan, B. D. Layer, and H. M. Milchberg, "Plasma waveguides efficiently generated by Bessel beams in elongated cluster gas jets," Phys. Rev. E **72**(3), 036411 (2005).

[54] B. D. Layer, A. G. York, S. Varma, Y.-H. Chen, and H. M. Milchberg, "Periodic index-modulated plasma waveguide," Opt. Express **17**(6), 4263–4267 (2009).

[55] S. J. Yoon, A. J. Goers, G. A. Hine, J. D. Magill, J. A. Elle, Y.-H. Chen, and H. M. Milchberg, "Shock formation in supersonic cluster jets and its effect on axially modulated laser-produced plasma waveguides," Opt. Express **21**(13), 15878–15887 (2013).

[56] F. Salehi, M. Le, L. Railing, M. Kolesik, and H. M. Milchberg, "Laser-accelerated, low-divergence 15-MeV quasimonoenergetic electron bunches at 1 kHz," Phys. Rev. X **11**(2), 021055 (2021).

[57] C. E. Clayton, J. E. Ralph, F. Albert, R. A. Fonseca, S. H. Glenzer, C. Joshi, W. Lu, K. A. Marsh, S. F. Martins, W. B. Mori, A. Pak, F. S. Tsung, B. B. Pollock, J. S. Ross, L. O. Silva, and D. H. Froula, "Self-guided laser wakefield acceleration beyond 1 GeV using ionization-induced injection," Phys. Rev. Lett. **105**(10), 105003 (2010).

[58] C. McGuffey, A. G. R. Thomas, W. Schumaker, T. Matsuoka, V. Chvykov, F. J. Dollar, G. Kalintchenko, V. Yanovsky, A. Maksimchuk, K. Krushelnick, V. Yu. Bychenkov, I. V. Glazyrin, and A. V. Karpeev, "Ionization induced trapping in a laser wakefield accelerator," Phys. Rev. Lett. **104**(2), 025004 (2010).

[59] M. Chen, E. Esarey, C. B. Schroeder, C. G. R. Geddes, and W. P. Leemans, "Theory of ionization-induced trapping in laser-plasma accelerators," Phys. Plasmas **19**(3), 033101 (2012).

[60] J. E. Shrock, "Multi-GeV laser wakefield acceleration in optically generated plasma waveguides," Ph.D. thesis (University of Maryland, 2023).

[61] "Ansys Fluent, Release 2023R2," AYSYS, Inc., 2023.

[62] D. F. Gordon, P. Sprangle, S. Slinker, R. Fernsler, and M. Lampe, *SPARC - A Simulation Model for Electrical Charges* (Defense Technical Information Center, Fort Belvoir, VA, 2006).

[63] J.-N. Vigneau, T.-T. N. Dang, and E. Charron, "Electro-nuclear dynamics of single and double ionization of H_2 in ultrafast intense laser pulses," J. Phys. Chem. A **128**(7), 1375–1384 (2024).

[64] J.-L. Vay, A. Huebl, A. Almgren, L. D. Amorim, J. Bell, L. Fedeli, L. Ge, K. Gott, D. P. Grote, M. Hogan, R. Jambunathan, R. Lehe, A. Myers, C. Ng, M. Rowan, O. Shapoval, M. Thévenet, H. Vincenti, E. Yang, N. Zaïm, W. Zhang, Y. Zhao, and E. Zoni, "Modeling of a chain of three plasma accelerator stages with the WarpX electromagnetic PIC code on GPUs," Phys. Plasmas **28**(2), 023105 (2021).

[65] R. Lehe, M. Kirchen, I. A. Andriyash, B. B. Godfrey, and J.-L. Vay, "A spectral, quasi-cylindrical and dispersion-free particle-in-cell algorithm," Comput. Phys. Commun. **203**, 66–82 (2016).

[66] B. A. Shadwick, C. B. Schroeder, and E. Esarey, "Nonlinear laser energy depletion in laser-plasma accelerators," Phys. Plasmas **16**(5), 056704 (2009).

[67] C. Benedetti, F. Rossi, C. B. Schroeder, E. Esarey, and W. P. Leemans, "Pulse evolution and plasma-wave phase velocity in channel-guided laser-plasma accelerators," Phys. Rev. E **92**(2), 023109 (2015).

[68] Y. Wang, S. Wang, A. Rockwood, B. M. Luther, R. Hollinger, A. Curtis, C. Calvi, C. S. Menoni, and J. J. Rocca, "0.85 PW laser operation at 3.3 Hz and high-contrast ultrahigh-intensity $\lambda = 400$ nm second-harmonic beamline," Opt. Lett. **42**(19), 3828–3831 (2017).

[69] P. Sprangle, B. Hafizi, J. R. Peñano, R. F. Hubbard, A. Ting, C. I. Moore, D. F. Gordon, A. Zigler, D. Kaganovich, and T. M. Antonsen, "Wakefield generation and GeV acceleration in tapered plasma channels," Phys. Rev. E **63**(5), 056405 (2001).

[70] W. Rittershofer, C. B. Schroeder, E. Esarey, F. J. Grüner, and W. P. Leemans, "Tapered plasma channels to phase-lock accelerating and focusing forces in laser-plasma accelerators," Phys. Plasmas **17**(6), 063104 (2010).

[71] E. Guillaume, A. Döpp, C. Thaury, K. Ta Phuoc, A. Lifschitz, G. Grittani, J.-P. Goddet, A. Tafzi, S. W. Chou, L. Veisz, and V. Malka, "Electron rephasing in a laser-wakefield accelerator," Phys. Rev. Lett. **115**(15), 155002 (2015).

[72] J. D. Ludwig, S. C. Wilks, A. J. Kemp, G. J. Williams, E. Rockafellow, B. Miao, J. E. Shrock, H. M. Milchberg, J.-L. Vay, A. Huebl, R. Lehe, S. S. Bulanov, A. Cimmino, P. Valenta, G. Grittani, R. Versaci, V. Tang, and B. Reagan, "Laser-based 100 GeV electron acceleration scheme for muon production," Sci. Rep. (submitted) (2025).

[73] B. B. Pollock, C. E. Clayton, J. E. Ralph, F. Albert, A. Davidson, L. Divol, C. Filip, S. H. Glenzer, K. Herpoldt, W. Lu, K. A. Marsh, J. Meinecke, W. B. Mori, A. Pak, T. C. Rensink, J. S. Ross, J. Shaw, G. R. Tynan, C. Joshi, and D. H. Froula, "Demonstration of a narrow energy spread, $\sim$0.5 GeV electron beam from a two-stage laser wakefield accelerator," Phys. Rev. Lett. **107**(4), 045001 (2011).

[74] K. G. Miller, J. R. Pierce, M. V. Ambat, J. L. Shaw, K. Weichman, W. B. Mori, D. H. Froula, and J. P. Palastro, "Dephasingless laser wakefield acceleration in the bubble regime," Sci. Rep. **13**, 21306 (2023).

[75] J. P. C. Cabadağ, R. Pausch, S. Schöbel, M. Bussmann, Y.-Y. Chang, S. Corde, A. Debus, H. Ding, A. Döpp, F. M. Foerster, M. Gilljohann, F. Haberstroh, T. Heinemann, B. Hidding, S. Karsch, A. Koehler, O. Kononenko, A. Knetsch, T. Kurz, A. M. de la Ossa, A. Nutter, G. Raj, K. Steiniger, U. Schramm, P. Ufer, and A. Irman, "Gas-dynamic density downramp injection in a beam-driven plasma wakefield accelerator," Phys. Rev. Res. **3**(4), L042005 (2021).

[76] C. G. R. Geddes, K. Nakamura, G. R. Plateau, C. Toth, E. Cormier-Michel, E. Esarey, C. B. Schroeder, J. R. Cary, and W. P. Leemans, "Plasma-density-gradient injection of low absolute-momentum-spread electron bunches," Phys. Rev. Lett. **100**(21), 215004 (2008).

[77] Z. Nie, C.-H. Pai, J. Hua, C. Zhang, Y. Wu, Y. Wan, F. Li, J. Zhang, Z. Cheng, Q. Su, S. Liu, Y. Ma, X. Ning, Y. He, W. Lu, H.-H. Chu, J. Wang, W. B. Mori, and C. Joshi, "Relativistic single-cycle tunable infrared pulses generated from a tailored plasma density structure," Nat. Photonics **12**(8), 489–494 (2018).

[78] Z. Nie, C.-H. Pai, J. Zhang, X. Ning, J. Hua, Y. He, Y. Wu, Q. Su, S. Liu, Y. Ma, Z. Cheng, W. Lu, H.-H. Chu, J. Wang, C. Zhang, W. B. Mori, and C. Joshi, "Photon deceleration in plasma wakes generates single-cycle relativistic tunable infrared pulses," Nat. Commun. **11**(1), 2787 (2020).

[79] S. Corde, K. Ta Phuoc, G. Lambert, R. Fitour, V. Malka, A. Rousse, A. Beck, and E. Lefebvre, "Femtosecond x rays from laser-plasma accelerators," Rev. Mod. Phys. **85**(1), 1–48 (2013).

[80] S. Steinke, J. van Tilborg, C. Benedetti, C. G. R. Geddes, C. B. Schroeder, J. Daniels, K. K. Swanson, A. J. Gonsalves, K. Nakamura, N. H. Matlis, B. H. Shaw, E. Esarey, and W. P. Leemans, "Multistage coupling of independent laser-plasma accelerators," Nature **530**, 190–193 (2016).